Meridional shifts in the marine ITCZ and the tropical hydrologic cycle over the last three glacial cycles

Matthew W. Schmidt[1] and Howard J. Spero[2]

Received 5 April 2010; revised 1 December 2010; accepted 23 December 2010; published 17 February 2011.

[1] Paleoproxy studies show a strong correlation between tropical climate and high-latitude temperature variability recorded in the Greenland ice cores over the last glacial cycle. In particular, abrupt cooling events in the Greenland Ice Sheet Project II $\delta^{18}O$ ice record appear synchronous with a southward migration of the Intertropical Convergence Zone (ITCZ) in the Atlantic, a weakening of the Indian and East Asian monsoon systems, and a strengthening of the South American monsoon system. Because this high-to-low-latitude climate teleconnection significantly alters the tropical hydrologic cycle around the globe, it plays a critical role in regulating global climate on glacial-interglacial time scales. We compare $\delta^{18}O_{seawater}$ reconstructions (a salinity proxy generated from previously published Mg/Ca and oxygen isotope data on *Globigerinoides ruber* (white var.)) obtained from western Caribbean core ODP 999A and western equatorial Pacific core 806B across the last three glacial cycles to show that systematic variations in surface salinity at these sites suggest the tropical Hadley cell hydrologic system undergoes systematic reorganizations that differ dramatically between warm interglacial and cold glacial periods. Furthermore, cross-spectral and phase angle analyses of the ice-volume-corrected Caribbean and western Pacific $\delta^{18}O_{SW}$ records reveal a 100 kyr frequency in both records that is almost 180° out of phase and a 23 kyr frequency that is nearly in phase. This results in the development of a very large $\delta^{18}O_{SW}$ gradient between the Caribbean and the western equatorial Pacific on glacial-interglacial time scales that is best explained by a southward shift in both the Atlantic and Pacific ITCZ during North Atlantic cold phases.

Citation: Schmidt, M. W., and H. J. Spero (2011), Meridional shifts in the marine ITCZ and the tropical hydrologic cycle over the last three glacial cycles, *Paleoceanography*, *26*, PA1206, doi:10.1029/2010PA001976.

1. Introduction

[2] Both paleoproxy [*Dykoski et al.*, 2005; *Peterson et al.*, 2000; *Wang et al.*, 2001, 2004, 2006; *Yuan et al.*, 2004] and GCM modeling studies [*Dahl et al.*, 2005; *Stouffer et al.*, 2006; *Zhang and Delworth*, 2005] show that the tropical hydrologic cycle undergoes significant changes on glacial-interglacial time scales. The mean position of the marine Intertropical Convergence Zone (ITCZ) is determined by latitudinal gradients in sea surface temperature (SST) [*Chiang and Bitz*, 2005], so the ITCZ shifts southward during cold periods in the North Atlantic when Atlantic meridional overturning circulation (AMOC) is reduced [*Broccoli et al.*, 2006; *Stouffer et al.*, 2006; *Vellinga and Wood*, 2002; *Vellinga and Wu*, 2004]. For this reason, AMOC changes have the potential to affect the tropical hydrologic cycle, resulting in global-scale reorganizations of atmospheric circulation patterns. Precisely dated speleothem records show that cold periods in the North Atlantic correlate to a weakening of the Indian and East Asian monsoon (EAM) systems [*Dykoski et al.*, 2005; *Wang et al.*, 2001; *Yuan et al.*, 2004] and an intensification of the South American monsoon (SAM) [*Cruz et al.*, 2005; *Wang et al.*, 2004, 2006]. In addition, some modeling studies show that a southward shift in the glacial ITCZ increases the net water vapor transport out of the North Atlantic basin [*Lohmann*, 2003; *Vellinga and Wu*, 2004] and may even alter the net transport of water vapor across the Central American isthmus [*Pahnke et al.*, 2007; *Xie et al.*, 2008], potentially altering the Atlantic-Pacific salinity gradient and thus affecting long-term changes in AMOC.

[3] Here, we compare a 350 kyr record of $\delta^{18}O_{seawater}$ ($\delta^{18}O_{SW}$; a salinity proxy) variability from Western Caribbean Ocean Drilling Program (ODP) Site 999A (12°45′N, 78°44′W; 2,827 m depth; 4 cm/kyr sed. rate) based on previously published $\delta^{18}O$ and Mg/Ca data [*Schmidt et al.*, 2006a] and initially presented by *Nürnberg et al.* [2008] with a similar $\delta^{18}O_{SW}$ reconstruction from ODP Site 806B (western equatorial Pacific (WEP); 0°19′N, 159°22′E; 2,520 m depth; 2 cm/kyr sed. rate)) [*Lea et al.*, 2000] that show two distinct modes of tropical hydrologic cycle dynamics across the last three glacial cycles. By examining $\delta^{18}O_{SW}$ change between these two distant sites, we identify an interglacial mode that is similar to today and a glacial mode that seems to be characterized by a more southerly position of the marine

[1]Department of Oceanography, Texas A&M University, College Station, Texas, USA.
[2]Department of Geology, University of California Davis, Davis, California, USA.

0883-8305/11/2010PA001976

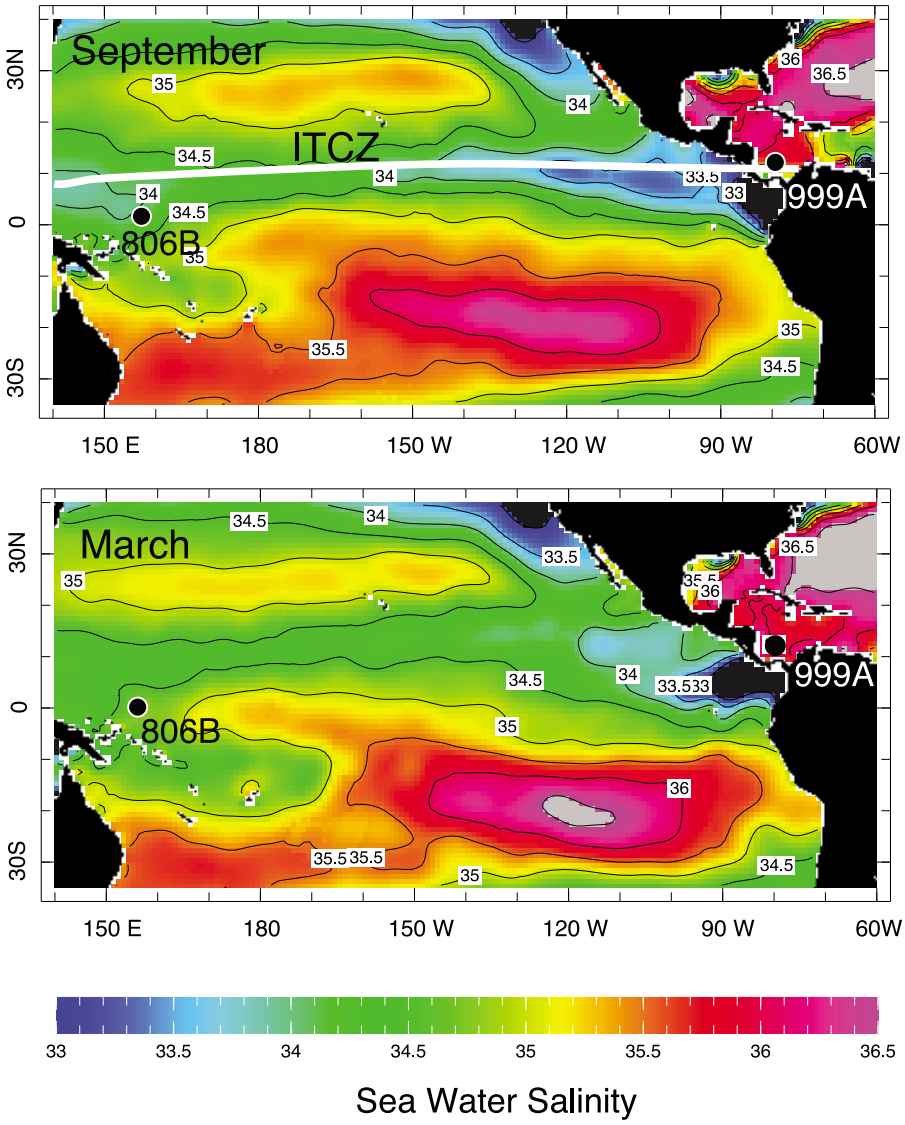

Figure 1. Average summer (September) and winter (March) SSS in the western tropical Atlantic and the tropical Pacific [*Conkright et al.*, 2002]. The location of ODP 999A (12°45′N, 78°44′W; 2,827 m; 4 cm/kyr sedimentation rate) in the Colombian Basin and ODP 806B (0°19′N, 159°22′E) in the western equatorial Pacific are indicated. In September, the position of the ITCZ is at ~10°N in the EEP and at ~8°N in the WEP, but its position is less defined during March. SSS maps created at http://iridl.ldeo.columbia.edu/SOURCES/.NOAA/.NODC/.WOA05/.

ITCZ. We show that these findings are consistent with coupled ocean-atmosphere general circulation models.

2. Modern Climatology in the Caribbean and Western Tropical Pacific

[4] ODP 999A is located in the western Caribbean's Colombian Basin (Figure 1). The site is directly influenced by the warm Caribbean Current and is ideally suited to reconstruct changes in southern Caribbean surface water hydrography [*Kameo et al.*, 2004; *Mora and Martinez*, 2005; *Schmidt et al.*, 2006a]. Net evaporation exceeds precipitation (E > P) in the Caribbean, resulting in a freshwater deficit of 150 cm/yr in the central Colombian Basin [*Curry et al.*, 2003]. However, unlike the Gulf of Mexico and the high-latitude North Atlantic, Caribbean sea surface salinity (SSS) is not significantly affected by freshwater runoff and therefore SSS primarily reflects the E-P distribution in the western tropical Atlantic.

[5] Climate in the modern Colombian Basin at 13°N is characterized by two distinct seasons: a warm, wet season in late summer when the ITCZ is located farthest to the north, and a cool, dry season during boreal winter when the ITCZ migrates southward [*Stidd*, 1967]. Under modern conditions in the tropical western Atlantic, the ITCZ extends as far north as the upper Amazon and Orinoco basins and to the

Costa Rica/Nicaragua border during the boreal summer, and as far south as the Amazon Basin and southern Colombia and Ecuador during boreal winter [*Poveda et al.*, 2006].

[6] Atmospheric circulation over the Caribbean is influenced by two low-level jets. The easterly San Andrés, located at 10°–12°N over the Caribbean, and the westerly Choco jet, located at 5°N over the eastern Pacific, both interact with the ITCZ to control regional precipitation patterns [*Magaña et al.*, 1999; *Poveda and Mesa*, 2000; *Poveda et al.*, 2006]. From December to February when the ITCZ is located farthest to the south, the northeast trade winds intensify, the San Andrés jet strengthens and precipitation over the Caribbean decreases. Conversely, when the northeast trade winds diminish, Caribbean precipitation increases and the low-level easterly jet weakens during boreal summer [*Poveda et al.*, 2006]. As a result, the modern annual SSS in the Colombian Basin varies by 0.5 practical salinity units (psu), attaining a minimum of 35.5 psu in September and a maximum of 36.0 psu in March (Figure 1) [*Conkright et al.*, 2002]. After flowing across the Caribbean and transporting water vapor over the Central American Isthmus, a segment of the jet then flows southeast over the Pacific and forms part of the Choco jet together with the cross-equatorial flow from the southern hemisphere [*Poveda et al.*, 2006]. Thus, the San Andrés jet forms an important atmospheric link between the Caribbean and the eastern Pacific [*Magaña et al.*, 1999; *Poveda et al.*, 2006].

[7] El Niño/Southern Oscillation (ENSO) variability also directly impacts modern climate in the tropical north Atlantic, resulting in reduced rainfall, warmer SSTs, and weaker trade winds in the western Tropical Atlantic during an El Niño event [*Alexander and Scott*, 2002; *Alexander et al.*, 2002; *Giannini et al.*, 2001; *Poveda and Mesa*, 1997]. Analysis of 40 years of data on the position of the ITCZ shows that its mean position is displaced southward during an El Niño phase, resulting in a rainfall deficit in Central America [*Hastenrath*, 2002]. Historic records show that El Niño events also result in increased tropical Atlantic aridity [*Poveda and Mesa*, 1997].

[8] ODP 806B is located on the Ontong Java Plateau in the heart of the western Pacific warm pool. Therefore, SSTs in this region of the Pacific are among the warmest waters on the planet and seasonal climate variability is relatively minimal. SST's typically exceed 29°C and vary by less than 1°C over the annual cycle [*Conkright et al.*, 2002]. Compared to the tropical Atlantic and eastern equatorial Pacific, ITCZ dynamics are much more complex in the WEP. Under modern conditions, the ITCZ migrates between three distinct locations over the course of the annual cycle. In the area between 130°E and 150°W, the ITCZ is located in a northern region (4°–10°N) for 37% of the year, in the equatorial region (4°N–4°S) for 3% of the year and in a southern region (4°–10°S) for 24% of the year [*Chen et al.*, 2008]. In addition, the ITCZ in the WEP also exists in a double mode (6% of the year) when deep convection takes place simultaneously in the northern and southern regions and in full mode where deep convection extends from 7°N to 10°S (5% of the year) [*Chen et al.*, 2008]. Finally, a weak or no ITCZ exists in the region for up to 25% of the year [*Chen et al.*, 2008]. From June through October, the ITCZ is more likely to be located north of site 806B in its northern position and from January through March it is more likely to be located south of the site in its southern position [*Chen et al.*, 2008]. As a result, annual SSS variability at site 806B is about 1 psu, ranging from a high of 35.0 psu during winter months to a low of 34.0 psu in September when the ITCZ is likely to be located just to the north of the site (Figure 1) [*Conkright et al.*, 2002].

[9] Site 806B is located near the eastern margin of the modern western Pacific warm pool [*Delcroix and Picaut*, 1998]. Therefore, zonal circulation changes associated with ENSO variability has mixed affects on SST and SSS changes at the site. In general, an El Niño event results in a SSS increase at the location of site 806B and a SSS decrease in the equatorial band east of site 806B from 150°E–140°W [*Delcroix and Picaut*, 1998]. Nevertheless, zonal shifts in the tropical Pacific during the strong 1997–1998 El Niño resulted in increased precipitation (and reduced SSS) in the western equatorial Pacific east of 160°E [*Delcroix and McPhaden*, 2002]. It is interesting that the equatorial decrease in SSS during the 1997–1998 El Niño is also associated with a southward migration of the Pacific ITCZ [*Delcroix and McPhaden*, 2002]. However, because the site is located near the eastern margin of the Pacific fresh pool under neutral conditions and near the western margin of the fresh pool during El Niño events, the site is not ideally located to monitor zonal changes in the Pacific associated with ENSO variability.

3. Materials and Methods

3.1. Geochemical Analyses

[10] Data and analytical methods for the ODP 999A and 806B reconstructions were presented previously by *Schmidt et al.* [2004, 2006a] and *Lea et al.* [2000]. Briefly, sediment from each core interval was disaggregated in ultrapure water, sieved and dried at room temperature. *G. ruber* were selected from the 250–350 μm size fraction. Stable isotope analyses were conducted on 25–30 shells/sample which were first sonicated in methanol for 3–8 s, roasted in vacuo at 375°C for 30 min, and then analyzed on a Micromass Optima Isotope Ratio Mass Spectrometer using an Isocarb common acid bath system at UC Davis.

[11] Sea surface temperatures were determined using Mg/Ca ratios measured on the same population and size fraction of *G. ruber* utilized for the δ^{18}O analyses. Approximately 600 μg of shell/sample (~60 shells) was cleaned for trace and minor element analysis without the DTPA step [*Lea et al.*, 2000; *Mashiotta et al.*, 1999] and rinsed in ultrapure water, and subsequently treated with hot reducing and oxidizing solutions and final leaches in a dilute ultrapure acid solution. Samples were then dissolved and analyzed on a Finnigan Element-2 ICPMS at UC Santa Barbara using procedures described by *Lea and Martin* [1996], *Mashiotta et al.* [1999], and *Lea et al.* [2000].

[12] For ODP 999A, Mg/Ca ratios were converted to SST (Figure 2c) utilizing the depth-corrected *G. ruber* Mg/Ca-SST

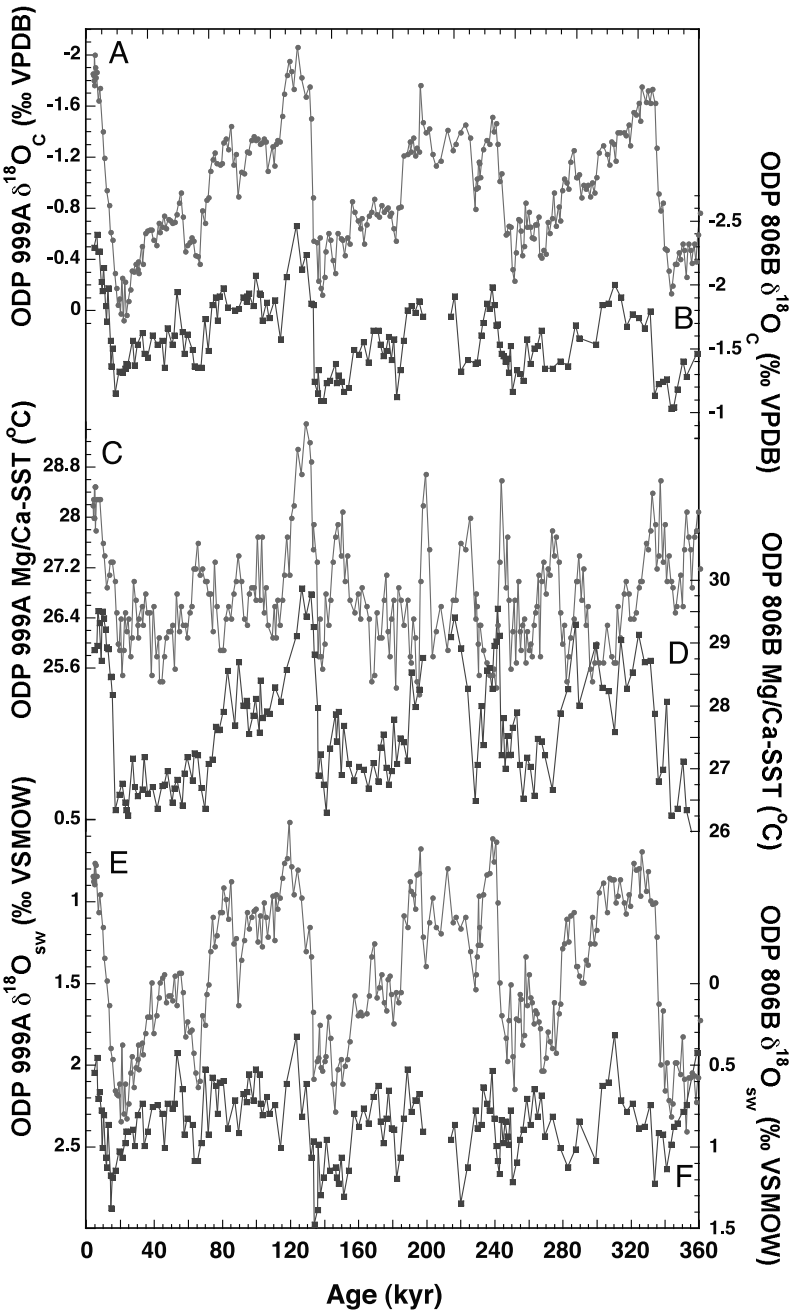

Figure 2. Measured *G. ruber* $\delta^{18}O_C$ from (a) Colombian Basin core ODP 999A [*Schmidt et al.*, 2006a] and (b) WEP core 806B [*Lea et al.*, 2000] over the past 360 kyr. SST records reconstructed using Mg/Ca ratios in *G. ruber* from (c) ODP 999A [*Schmidt et al.*, 2006a] and (d) 806B [*Lea et al.*, 2000]. Computed $\delta^{18}O_{SW}$ calculated from Mg/Ca-derived SST and $\delta^{18}O_C$ for (e) ODP 999A [*Schmidt et al.*, 2006a] and (f) 806B [*Lea et al.*, 2000]. Note that the amplitude of the calculated $\delta^{18}O_{SW}$ change in the Colombian Basin is considerably greater than the calculated $\delta^{18}O_{SW}$ change in the WEP.

calibration for the tropical Atlantic [*Dekens et al.*, 2002] where depth equaled 2.8 km:

$$\mathrm{Mg/Ca} = 0.38\ \exp 0.09[\mathrm{SST} - 0.61(\text{water depth km})]. \quad (1)$$

SSTs for core 806B (Figure 2d) were calculated using the depth-corrected *G. ruber* Mg/Ca-SST calibration for the tropical Pacific [*Dekens et al.*, 2002] where depth equaled 2.5 km:

$$\mathrm{Mg/Ca} = 0.38\ \exp 0.09[\mathrm{SST} - 0.61(\text{water depth km}) - 1.6]. \quad (2)$$

To compute $\delta^{18}O_{SW}$, temperature was removed from the $\delta^{18}O_{calcite}$ records (Figures 2a and 2b) using a temperature-$\delta^{18}O$ relationship that has been field calibrated for use with *G. ruber* (white) (Figures 2e and 2f) [*Bemis et al.*, 1998; *Thunell et al.*, 1999]:

$$T = 16.5 - 4.80\left(\delta^{18}O_C - \left(\delta^{18}O_{SW} - 0.27‰\right)\right). \quad (3)$$

[13] On glacial time scales, $\delta^{18}O_{SW}$ is also affected by variations in continental ice volume because the growth of continental ice sheets reflects the influence of Rayleigh fractionation which increases oceanic $\delta^{18}O_{SW}$. We therefore use the global $\delta^{18}O_{SW}$ record of *Waelbroeck et al.* [2002] to remove global ocean $\delta^{18}O_{SW}$ change from the records presented here.

[14] Seasonal foraminifera flux data from sediment traps are not available for the western Caribbean. However, a sediment trap study from the WEP showed that *G. ruber* flux in this region is at a maximum from mid-July through September [*Kawahata et al.*, 2002], suggesting that paleoreconstructions based on this species may be biased toward the summer months. Based on the comparison of the core top Mg/Ca-SST reconstruction from ODP 999A with modern seasonal SSTs in the western Caribbean, *Schmidt et al.* [2006b] concluded that the *G. ruber* reconstructions from the Caribbean are also biased toward summer months. We assume that the seasonal distribution and flux of *G. ruber* (white) was similar between the Western Caribbean Site 999A and western equatorial Pacific site 806B across the past three glacial cycles in the following discussions and comparisons [e.g., *Schmidt et al.*, 2006b].

3.2. Error Analysis

[15] Analytical precision for the $\delta^{18}O_C$ measurements from the ODP 999A record is better than ±0.06‰ (1σ). Mg/Ca analytical reproducibility for ODP 999A, determined by the analysis of consistency standards matched in concentration and Mg/Ca ratio to dissolved foraminifera solutions, is estimated at ±0.7% (1σ). The pooled standard deviation of replicate Mg/Ca analyses from ODP 999A is ±1.9% (1 SD, df = 324) based on 348 analyzed intervals. The overall precision of replicates at this site was slightly better than other tropical cores (typically ~3%) [*Lea et al.*, 2000, 2003], and most likely reflects the stability of the water column in the Colombian Basin during the last 360 kyr. Standard deviation for the $\delta^{18}O_{SW}$ residual was calculated to be ±0.22‰ using Monte Carlo methodology that assumes a ±1σ normal distribution in the $\delta^{18}O_C$ and Mg/Ca measurements and in the Mg/Ca-SST and $\delta^{18}O$-SST calibrations. In brief, we calculated the Monte Carlo error estimation by first generating a normal distribution of data using the reported error on our average Mg/Ca and $\delta^{18}O_{calcite}$ measurements. Then, a normal distribution of SSTs were generated using randomly selected Mg/Ca ratios from the first step above and using the 1σ reported error on the Mg/Ca-SST relationship from *Dekens et al.* [2002]. Finally, a normal distribution of $\delta^{18}O_{SW}$ values was generated using the 1σ error from the *Bemis et al.* [1998] SST: $\delta^{18}O_{calcite}$ relationship with randomly selected SST and $\delta^{18}O_{calcite}$ values from the steps above. We then calculated the 1σ error on the resulting $\delta^{18}O_{SW}$ data population, arriving at the estimated error of ±0.22‰. Using a variety of methods, previous studies report similar error propagations for the $\delta^{18}O_{SW}$ residual based on $\delta^{18}O_C$ and Mg/Ca-SSTs in *G. ruber*, ranging from ±0.18‰ to ±0.26‰ [*Carlson et al.*, 2008; *Lea et al.*, 2000; *Lund and Curry*, 2006; *Oppo et al.*, 2009; *Weldeab et al.*, 2006].

3.3. Age Models

[16] The previously published age models for ODP 999A [*Schmidt et al.*, 2004] and 806B [*Lea et al.*, 2000] are used in this study. Both age models were developed by tuning their respective *G. ruber* $\delta^{18}O_C$ records to SPECMAP [*Bassinot et al.*, 1994].

4. Results and Discussion

4.1. Western Caribbean and Western Equatorial Pacific $\delta^{18}O_{SW}$ During the Past 360 kyr

[17] The *G. ruber* $\delta^{18}O_C$ and Mg/Ca-SST records from ODP 999A [*Schmidt et al.*, 2006a] and 806B [*Lea et al.*, 2000] span three complete glacial cycles over the past 360 kyr (Figure 2). For the Late Holocene, we calculate an average western Caribbean $\delta^{18}O_{SW}$ value of 0.8‰ (Figure 2e) and an average WEP $\delta^{18}O_{SW}$ value of 0.5‰ (Figures 2e and 2f), in close agreement with modern $\delta^{18}O_{SW}$ estimates of 0.80–0.90‰ for the southwestern Caribbean and 0.3–0.4‰ for the WEP near site 806B [*Watanabe et al.*, 2001; G. A. Schmidt et al., Global Seawater Oxygen-18 Database, 1999, http://data.giss.nasa.gov/o18data/]. The $\delta^{18}O_{SW}$ record from site 999A has a maximum glacial-interglacial amplitude of ~1.6‰ across Termination I (TI), TII, and TIV, and a minimum amplitude of 1.5‰ across TIII. This glacial-interglacial $\delta^{18}O_{SW}$ amplitude exceeds estimates of global $\delta^{18}O_{SW}$ change due to continental ice volume variability by up to 0.5‰ [*Waelbroeck et al.*, 2002]. In comparison, the calculated $\delta^{18}O_{SW}$ change in the WEP at site 806B is less than the global $\delta^{18}O_{SW}$ change due to continental ice volume variability. Glacial-interglacial amplitudes of $\delta^{18}O_{SW}$ change at site 806B range from 0.6 to 0.7‰ across TI and TIII to ~1.0‰ across TII.

[18] We recognize that several lines of evidence have demonstrated that the Mg/Ca paleothermometer could be sensitive to ambient salinity [*Arbuszewski et al.*, 2009; *Ferguson et al.*, 2008] and that foraminifera shells are heterogeneous with respect to Mg [*Eggins et al.*, 2004; *Sadekov et al.*, 2008, 2009]. If correct, these issues might compromise our ability to reconstruct $\delta^{18}O_{sw}$ using Mg/Ca data. However, two lines of evidence argue against a significant salinity effect on Mg/Ca. First, culturing experiments have quantified the impact of salinity on *Orbulina universa* Mg/Ca and demonstrated that the effect is much smaller than proposed from field data (only 4% increase in Mg/Ca for a 1 psu increase in salinity) within the normal salinity range of Pacific and Atlantic surface waters. Furthermore, the Mg/Ca increase predicted for the LGM due to increased glacial ocean salinity is offset by the impact of pH on shell Mg/Ca ratios during glacial times (6% decrease in Mg/Ca for a 0.1 pH increase) [*Lea et al.*, 1999]. Second, a study of

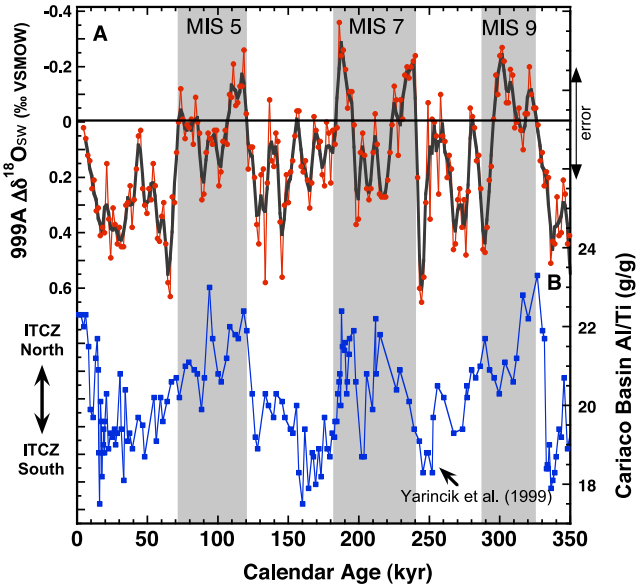

Figure 3. (a) The ice volume free $\Delta\delta^{18}O_{IVF\text{-}SW}$ record for ODP 999A, calculated by subtracting global $\delta^{18}O_{SW}$ change due to continental ice volume variability [*Waelbroeck et al.*, 2002] and the modern local $\delta^{18}O_{SW}$ value of 0.8‰. The error bar represents the estimated error on our calculated $\delta^{18}O_{SW}$ values of ±0.22‰ and as described in section 3.2. The $\Delta\delta^{18}O_{IVF\text{-}SW}$ record represents regional hydrologic changes in the Caribbean through the last three glacial cycles. The bold black line is a three-point running mean through the raw data (fine red line). (b) The Cariaco Basin Al/Ti record [*Yarincik et al.*, 2000], indicating a southern migration of the ITCZ (lower Al/Ti ratios) during glacial periods.

G.ruber from the high-salinity environment of the Red Sea showed that elevated Mg/Ca ratios were not caused by increased Mg uptake into foraminiferal calcite in a high-salinity setting (e.g., beyond those predicted by culturing studies), but rather resulted from secondary high Mg-calcite overgrowths that likely formed near the sediment-seawater interface [*Hoogakker et al.*, 2009]. Additional research is required to fully explain data that argue for a salinity effect on the Mg/Ca paleothermometer at elevated salinities. Interestingly, elevated Mg/Ca ratios are only seen in foraminifera growing at higher salinities. If this is a physiological response of foraminifera growing near the edge of their natural salinity range, then the effect may not influence the Mg/Ca ratio of open ocean glacial age foraminifera which would have been adapted to higher oceanic salinities as a result of continental ice growth.

[19] Intrashell Mg/Ca heterogeneity has been observed in planktonic foraminifera by a number of researchers [*Eggins et al.*, 2004; *Sadekov et al.*, 2008, 2009], raising concerns that additional complexity could influence Mg/Ca paleothermometry. However, recent laser ablation data on cultured foraminifera [*Spero et al.*, 2008] demonstrate that Mg/Ca heterogeneity in *Orbulina universa* is a natural component of shell growth related to day/night calcification as proposed by *Eggins et al.* [2004]. Furthermore, data demonstrate that both day and night calcite respond similarly to temperature by changing shell Mg/Ca. Because existing calibrations were generated by dissolving and analyzing all phases, thereby averaging intrashell Mg/Ca ratios from a suite of shells, intrashell heterogeneity should not impact our ability to reconstruct temperatures with this proxy.

[20] When the influence of continental ice volume [*Waelbroeck et al.*, 2002] and modern Caribbean surface $\delta^{18}O_{SW}$ value are subtracted, we obtain an ice volume free residual, $\Delta\delta^{18}O_{IVF\text{-}SW}$ (Figure 3a) that is normalized to the modern Caribbean. Positive values (e.g., $\Delta\delta^{18}O_{IVF\text{-}SW} >$ 0‰) indicate elevated SSS relative to the modern, due to the excess removal of ^{16}O-depleted water vapor via evaporation. In the western Caribbean, $\Delta\delta^{18}O_{IVF\text{-}SW}$ was more positive than modern seawater by ~0.5 to 0.6‰ during cold marine isotope stages (MIS) 2, 4, 6, 8, and 10. In contrast, during warm interglacial intervals MIS 3, 5, 7, and 9, $\delta^{18}O_{SW}$ is indistinguishable from, or slightly fresher than, average modern Colombian Basin surface $\delta^{18}O_{SW}$ (e.g., $\Delta\delta^{18}O_{IVF\text{-}SW} \approx 0$‰).

[21] The only difference between the $\Delta\delta^{18}O_{IVF\text{-}SW}$ we show in Figure 3a and the original calculation of the ODP 999A $\Delta\delta^{18}O_{IVF\text{-}SW}$ record published by *Nürnberg et al.* [2008] is the use of different Mg/Ca-SST calibrations. While *Nürnberg et al.* [2008] used the "all planktonic species" calibration of *Anand et al.* [2003] to calculate SSTs in both the ODP 999A (Colombian Basin) and the MD02-2575 (DeSoto Canyon, northeastern Gulf of Mexico) cores, we apply the depth-corrected Atlantic *G. ruber* calibration published by *Dekens et al.* [2002] to calculate downcore SST change at site 999A. Whereas both equations have the same preexponential and exponential constants, the *Dekens et al.* [2002] calibration has a depth correction for cores deeper than 2.5 km. However, use of the depth correction factor on ODP 999A results in calculated SSTs that are 1.0°C warmer and $\delta^{18}O_{SW}$ values that are 0.23‰ higher than previously published.

[22] Whereas these data indicate Caribbean salinities were elevated during cold glacial intervals, a conversion of $\delta^{18}O_{SW}$ to salinity is confounded by uncertainties in the slope of the relationship between these two variables at times in the past [*LeGrande and Schmidt*, 2009]. Nevertheless, if we assume the $\delta^{18}O_{SW}$:SSS relationship in the southwestern Colombian Basin during the last three glacial cycles was similar to the modern relationship [*Watanabe et al.*, 2001]

$$\delta^{18}O_{SW} = 0.22 \times SSS - 6.95, \quad (4)$$

then average glacial-interglacial $\Delta\delta^{18}O_{IVF\text{-}SW}$ change suggests orbital-scale surface salinity enrichments of between 2.3 and 2.7 psu during cold glacial periods. Although coupled ocean-atmosphere GCM simulations suggest little or no change in the $\delta^{18}O_{SW}$:SSS relationship during the LGM [*Roche et al.*, 2004], it is likely that the slope of this relationship was slightly greater than the modern during glacial times due elevated evaporation rates under more arid conditions (reduced glacial humidity). Increasing the slope of the $\delta^{18}O_{SW}$:SSS relationship reduces our computed glacial-interglacial SSS change in the Colombian Basin. Further-

more, an increase in glacial Caribbean SSS is in agreement with previous research that also found elevated western tropical Atlantic SSS during glacial periods [*Dürkoop et al.*, 1997]. Therefore, it seems likely that the elevated surface salinities extended beyond the Caribbean and probably reflects a regional pattern of elevated E-P values in the western tropical north Atlantic.

4.2. ITCZ Influence on Tropical Atlantic Salinity

[23] Comparison of the Caribbean ODP 999A $\Delta\delta^{18}O_{IVF\text{-}SW}$ record with the Cariaco Basin Al/Ti record over the last 350 kyr [*Yarincik et al.*, 2000] shows that elevated Caribbean salinities correspond to reduced Al/Ti ratios (Figure 3b). *Yarincik et al.* [2000] argued that reduced Cariaco Al/Ti ratios during glacial periods result from increased eolian input from the northern Sahara Desert, suggesting a strengthening of glacial trade winds in the northern Hemisphere and a more arid northern tropical Atlantic. Although the Cariaco Basin Al/Ti record was sampled at a lower resolution than our Caribbean record over the last 350 kyr (Figure 3) and thus does not record the same detail, the comparison suggests that the more southerly glacial ITCZ corresponds to periods of elevated SSS in the Caribbean. In a comparable study, *Mora and Martinez* [2005] recorded lower glacial Al/Ti and K/Ti ratios in sediments from ODP 999A over the past four glacial cycles, suggesting reduced glacial riverine input into the Colombian Basin by the Magdalena River and a more arid glacial Caribbean climate. In addition, the Cariaco Basin Al/Ti and the ODP 999A Al/Ti and K/Ti records all display large glacial-interglacial amplitudes with 100 kyr cyclicities, suggesting links between northern hemisphere ice sheet volume and the mean position of the ITCZ in the tropical Atlantic [*Mora and Martinez*, 2005; *Yarincik et al.*, 2000].

[24] General circulation model (GCM) simulations suggest that the tropical hydrologic cycle responds to longer-scale changes in northern hemisphere climate. Modeling results show that cooling in the North Atlantic associated with weak AMOC results in a southward shift in the mean annual position of the ITCZ, an intensification of the North Atlantic subtropical atmospheric high-pressure cell, enhanced water vapor removal from the north Atlantic subtropical gyre and increased freshwater input into the south Atlantic [*Vellinga and Wood*, 2002; *Lohmann*, 2003; *Vellinga and Wu*, 2004; *Dahl et al.*, 2005; *Zhang and Delworth*, 2005; *Lohmann and Lorenz*, 2000; *Stouffer et al.*, 2006]. Modeling studies also suggest the Atlantic ITCZ is especially sensitive to land and sea ice cover in the Northern Hemisphere [*Chiang et al.*, 2003; *Chiang and Bitz*, 2005]. These studies provide a mechanism that explains how the meridional migration of the Atlantic ITCZ can be forced by changes in the strength of AMOC which can, in turn, result in atmospheric feedback responses. These atmospheric feedbacks may reduce the amount of freshwater precipitation into the tropical and subtropical North Atlantic while increasing atmospheric freshwater export out of the basin.

4.3. ENSO Variability and Caribbean $\delta^{18}O_{SW}$

[25] Although there is still considerable debate about ENSO variability during glacial times, several paleo-proxy studies suggest the average glacial state of the tropical Pacific was characterized by more permanent El Niño–like conditions [*Koutavas et al.*, 2002; *Koutavas and Lynch-Stieglitz*, 2003; *Stott et al.*, 2002]. For instance, *Koutavas et al.* [2002] found a reduction in the cross-equatorial SST gradient in the eastern equatorial Pacific during the LGM, and *Stott et al.* [2002] presented a record of $\delta^{18}O_{SW}$ change near Indonesia indicating elevated glacial surface salinity in the WEP.

[26] Coupled GCM results using LGM boundary conditions (including ice sheet reconstructions) also show a simulated increase in frequency and a decrease in the amplitude of ENSO events during the LGM [*Bush*, 2007]. Based on another GCM experiment, *Dong and Sutton* [2007] found that cooling in the North Atlantic associated with a significant AMOC reduction had a strong effect on ENSO variability. In particular, atmospheric teleconnections associated with a weakened AMOC state resulted in a southward migration of the ITCZ, stronger ENSO variability and a strengthening of El Niño events [*Dong and Sutton*, 2007]. Other modeling studies point to tropical insolation variability as playing a major role in driving changes in the tropical hydrologic cycle [*Bush and Philander*, 1998; *Cane and Clement*, 1999; *Cane*, 1998; *Clement and Cane*, 1999; *Kukla et al.*, 2002]. These studies showed that orbitally-driven changes in the amount of seasonal solar insolation at the equator influences ENSO variability in the Pacific, correlating warm periods (Early Holocene and MIS 5e) with enhanced La Niña circulation and continental ice growth with stronger El Niño forcing [*Clement et al.*, 1999; *Kukla et al.*, 2002]. According to this model, changes in the seasonal distribution of insolation at the equator, measured as the March to September insolation difference on the equator, results in stronger El Niño forcing in the tropical Pacific (Figure 4) [*Clement et al.*, 1999; *Kukla et al.*, 2002]. When this index was high during the LGM and MIS 4, 6, 8, and 10, this model suggests that El Niño events would have been more frequent. Conversely, as this index decreases and summer insolation exceeds winter insolation, the annual cycle in the tropical Pacific was amplified and the model suggests that La Niña events were more frequent.

[27] Comparison of the Caribbean ice volume free $\delta^{18}O_{SW}$ record with this insolation forcing index over the last 360 kyr (Figure 4) shows a close agreement over much of the record, suggesting that elevated $\delta^{18}O_{SW}$ values correlate to periods when El Niño forcing was at a maxima (i.e., the LGM, MIS 4, the glacial maximum at MIS 6, and MIS 8). Furthermore, the lowest $\delta^{18}O_{SW}$ values in the record occur when the model suggests La Niña forcing would have been strongest during MIS 5e, 7a, 7e, and 9. In addition, there are two glacial period offsets (during MIS 3 and MIS 6) between the site 999A $\Delta\delta^{18}O_{IVF\text{-}SW}$ record and the ENSO forcing index (Figure 4). These offsets occur at times when the ENSO index suggests stronger El Niño forcing, but $\delta^{18}O_{IVF\text{-}SW}$ record suggests fresher conditions, more typical of a La Niña circulation pattern. It is interesting that these intervals both occur during transitional periods during the last two glacial cycles, just after periods of major ice sheet expansion (MIS 4 and the early phase of MIS 6), but before the development of maximum glacial conditions (the LGM

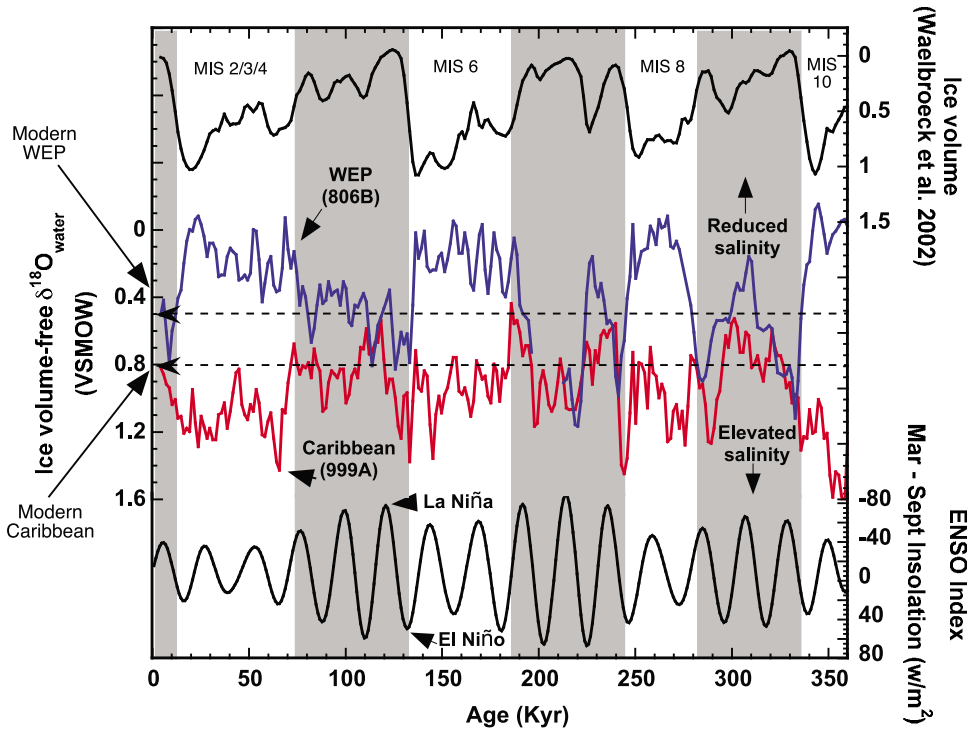

Figure 4. Computed $\delta^{18}O_{IVF\text{-}SW}$ record from western Caribbean ODP 999A (red line) and western equatorial Pacific core ODP 806B (blue line) [*Lea et al.*, 2000]. Both records have been smoothed by interpolation to a 1.5 kyr time interval. The modern $\delta^{18}O_{SW}$ values for each site are indicated by the dashed lines. Note that the $\delta^{18}O_{IVF\text{-}SW}$ gradient between the Caribbean and the WEP is reduced during interglacials and increases during glacial periods. The top portion shows the continental ice volume $\delta^{18}O_{SW}$ reconstruction from *Waelbroeck et al.* [2002] (black line) illustrating that the Caribbean-WEP surface salinity gradient covaries with changes in continental ice volume. The bottom portion shows changes in the seasonal distribution of insolation at the equator, measured as the March to September difference on the equator and calculated using information from *Paillard et al.* [1996]. El Niño forcing is stronger when this difference increases [*Clement et al.*, 1999; *Kukla et al.*, 2002]. Grey bars indicate interglacial periods.

and the penultimate glacial maximum at ~136 kyr). Additional climate forcing mechanisms may have complicated the affects of ENSO variability on tropical Atlantic climate during these periods of milder climate in the middle of the last two glacial cycles.

[28] It is also possible that glacial periods may have been characterized by a weaker, but more permanent El Niño–like circulation pattern. As such, this shift in the tropical hydrologic cycle to more frequent glacial El Niño–like modes would have reinforced the effects of a more southerly position of the ITCZ during periods of reduced AMOC, resulting in a feedback that increased the salinity of the north Atlantic, thus priming the North Atlantic gyre for a rapid return to an interglacial circulation mode of more vigorous AMOC. This conclusion is in agreement with coupled ocean-atmosphere GCM results [*Latif et al.*, 2000; *Schmittner and Clement*, 2002] and a data reanalysis study [*Schmittner et al.*, 2000] indicating that modern atmospheric circulation patterns associated with an El Niño result in enhanced water vapor removal from the tropical Atlantic.

4.4. Caribbean–Western Equatorial Pacific $\delta^{18}O_{SW}$ Difference

[29] Comparison of the Caribbean $\Delta\delta^{18}O_{IVF\text{-}SW}$ and WEP $\Delta\delta^{18}O_{IVF\text{-}SW}$ records demonstrates that interglacial Caribbean $\delta^{18}O_{SW}$ values are similar to, or more positive than, WEP $\delta^{18}O_{SW}$ values (Figure 4). Today, the mean contrast between Sites 999A and 806B SSS and $\delta^{18}O_{sw}$ is ~1.3 psu and 0.3‰, respectively. In contrast, Caribbean $\delta^{18}O_{SW}$ values become much more positive than WEP $\delta^{18}O_{SW}$ during cold glacial intervals, thereby increasing the interhemispheric $\delta^{18}O_{SW}$ gradient between these two locations to as much as 1.3‰ (Figure 4). As a result, glacial-interglacial $\delta^{18}O_{SW}$ changes are antiphased between sites 999A and 806B. The $\delta^{18}O_{SW}$ differences between sites covary with glacial-interglacial climate states as reconstructed by *Waelbroeck et al.* [2002] (Figure 4) and appear to be coupled during orbital-scale shifts in tropical atmospheric circulation, most likely resulting from meridional shifts in the mean position of the ITCZ and zonal shifts associated with ENSO variability. Although the resolution of these cores precludes our ability to

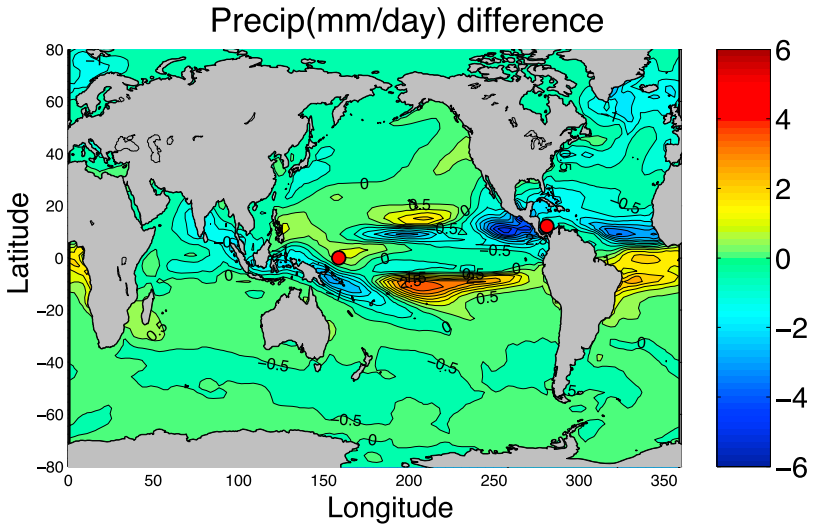

Figure 5. Modeling results after the coupled GCM experiment of *Zhang and Delworth* [2005] showing daily mean precipitation anomalies (millimeters per day) resulting from a reduction in AMOC caused by 0.6 Sv freshwater input into the northern North Atlantic. Also shown are the locations of ODP 999A in the western Caribbean and ODP 806B in the western equatorial Pacific (red circles). Note the negative precipitation anomaly in the Caribbean and the positive anomaly in the western North Pacific near site 806B due to a southward displacement of the marine ITCZ and an enhancement of Walker circulation in the north tropical Pacific. These results are consistent with the observed glacial-interglacial changes in the Caribbean-WEP $\delta^{18}O_{IVF\text{-}SW}$ records.

evaluate millennial-scale shifts in the ITCZ, these results suggest that the Caribbean-WEP $\delta^{18}O_{SW}$ gradient oscillates between two fundamental modes; an interglacial mode where the gradient is relatively small as the mean position of the ITCZ shifts northward and a glacial mode where the Caribbean becomes significantly saltier than the WEP and the ITCZ is in a more southerly position.

[30] Speleotherm records from Borneo (4°N) [*Partin et al.*, 2007] support these conclusions and show that the western tropical Pacific north of the equator was drier during the LGM. After experiencing the driest conditions during Heinrich Event 1, Borneo speleothems indicate the ITCZ began to migrate northward through the deglacial, finally reaching 4°N over Borneo at 5 kyr [*Partin et al.*, 2007]. Because site 806B is located southeast of these speleothem records on the equator, it is possible that the equatorial zone spent a much greater period of time under the ITCZ during the glacial than at present. Alternatively, if Walker circulation in the glacial tropical Pacific was more El Niño–like, atmospheric convection may have shifted eastward away from Borneo and closer to the central Pacific, resulting in more freshwater precipitation at site 806B. Based on $\delta^{18}O_{SW}$ reconstructions from the eastern margin of the Indonesian archipelago, *Stott et al.* [2002] hypothesized that an eastern shift in the western Pacific rain belts resulted in increased glacial SSS in the Mindanao Sea.

[31] Although we cannot distinguish between mechanisms for glacial freshening at site 806B, we believe meridional shifts in the ITCZ played an important role. Today, the ITCZ in the WEP is only located in the equatorial region for 3.2% of the year, but is located in the northern region from 4°–10°N for 37% of the year between June and October [*Chen et al.*, 2008]. If this northern extreme position shifted southward during the LGM, the equatorial region around 806B would have experienced more rainfall. *Sachs et al.* [2009] also provide proxy evidence demonstrating how a similar southward shift in the ITCZ during the Little Ice Age had a dramatic effect on the latitudinal distribution of precipitation in the central Pacific. Their results support the idea of a near-equatorial position for the marine ITCZ during the Little Ice Age. Likewise, new reconstructions of $\delta^{18}O_{SW}$ and organic biomarkers from the Indo-Pacific Warm Pool also found evidence for centennial-scale hydrologic changes associated with ITCZ migration over the past two millennia [*Oppo et al.*, 2009; *Tierney et al.*, 2010].

[32] Based on a fully coupled ocean-atmosphere global general circulation model experiment, *Zhang and Delworth* [2005] showed that a freshwater forcing of 0.6 Sv distributed over the northern North Atlantic results in a southward shift of the ITCZ over the tropical Atlantic (Figure 5), consistent with many other model simulations during Greenland stadials [*Stouffer et al.*, 2006; *Vellinga and Wood*, 2002]. Furthermore, their experiments show the Atlantic Hadley cell also shifts southward, resulting in a descending branch located at 10°N (resulting in reduced precipitation at site ODP 999A) and a near-surface ascending branch at the equator (increasing precipitation at ODP site 806B). *Zhang and Delworth* [2005] showed that the central Pacific ITCZ weakens in the north and strengthens in the south, becoming more symmetric about the equator. As AMOC weakens, a southern shift of the Pacific ITCZ increases freshwater precipitation on the equator at site 806B.

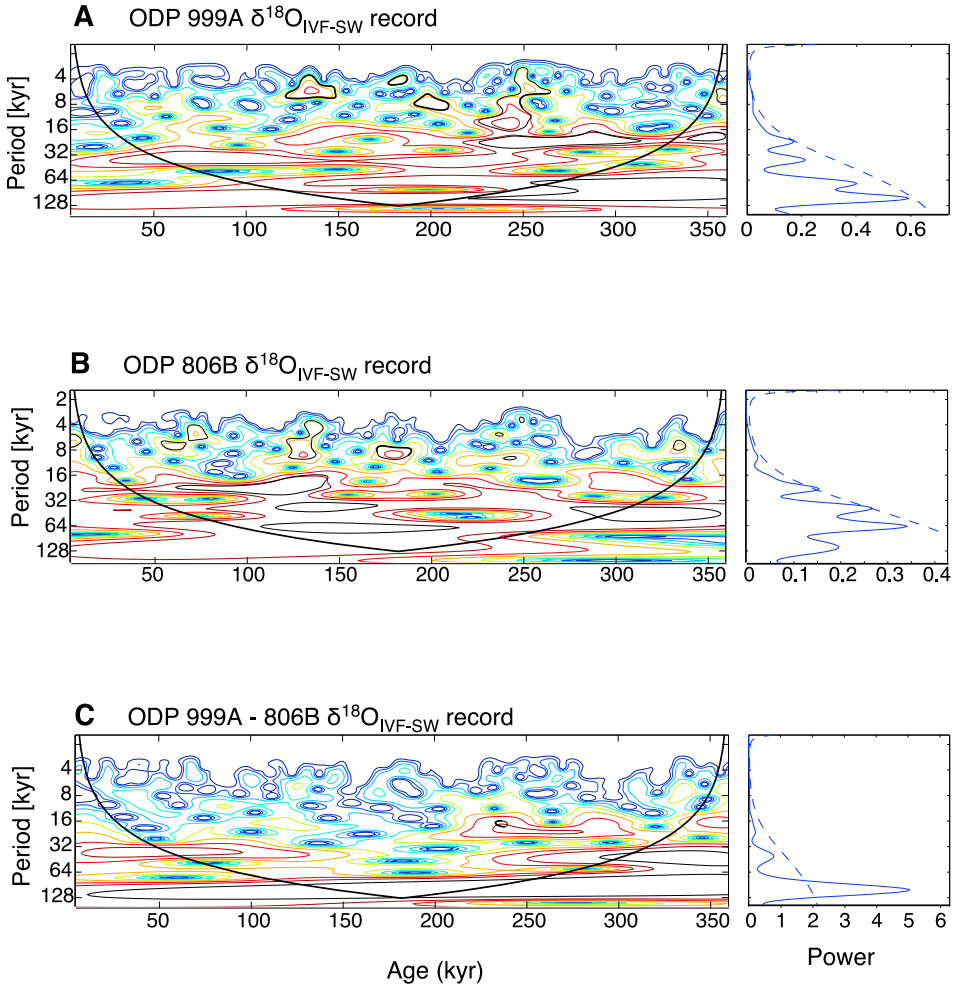

Figure 6. (left) Wavelet analysis and (right) power spectrum of the (a) ODP 999A $\delta^{18}O_{IVF\text{-}SW}$ record, (b) the 806B $\delta^{18}O_{IVF\text{-}SW}$ record, and (c) the difference of the ODP 999A − 806B $\delta^{18}O_{IVF\text{-}SW}$ records over the last 360 kyr. Warm colors indicate high spectral power in the wavelet analyses, and cool colors indicate low spectral power. Units are log-squared units per cycle per kiloyear. The black line on the wavelet analyses is the confidence boundary and the dashed black lines on the power spectrum indicate the 95% confidence level.

4.5. Spectral Analyses

[33] In order to explore the temporal evolution of frequencies in the ODP 999A and the 806B $\delta^{18}O_{IVF\text{-}SW}$ records, wavelet and power spectra analyses were generated using the methods outlined by *Torrence and Compo* [1998] (Figure 6). The ODP 999A $\delta^{18}O_{IVF\text{-}SW}$ power spectrum indicates 23 and 100 kyr frequencies at the 95% confidence level. In addition, the 999A wavelet analysis indicates high spectral power at the 41 kyr frequency in the younger part of the record until about 150 kyr and again between 170 and 270 kyr. Although below the 95% confidence level, the 999A $\delta^{18}O_{IVF\text{-}SW}$ record also contains power at the 60 kyr frequency. In comparison, the 806B power spectrum indicates statistically significant frequencies at 23, 41 and 60 kyr, in addition to a peak at the 100 kyr frequency just below the 95% confidence level. Although the 999A $\delta^{18}O_{IVF\text{-}SW}$ record contains slightly more spectral power at the precessional frequency, the presence of statistically significant spectral power at the 23 kyr frequency in both records most likely reflects the strong influence of precessional insolation variability on the tropical hydrologic cycle. When precessional insolation was high in the Northern Hemisphere tropics and the annual cycle at a maximum, the intensity of atmospheric convection associated with the ITCZ probably also increased at both sites.

[34] Next, we subtracted the 806B $\delta^{18}O_{SW}$ record from the 999A $\delta^{18}O_{SW}$ record (thereby removing ice volume) and performed a wavelet analysis on the difference in $\delta^{18}O_{SW}$ between the two sites (Figure 6c). Results indicate only the 100 kyr frequency is greater than the 95% confidence level. If the 100 kyr cycle is out of phase between the two sites, then spectral power at this frequency would be amplified in

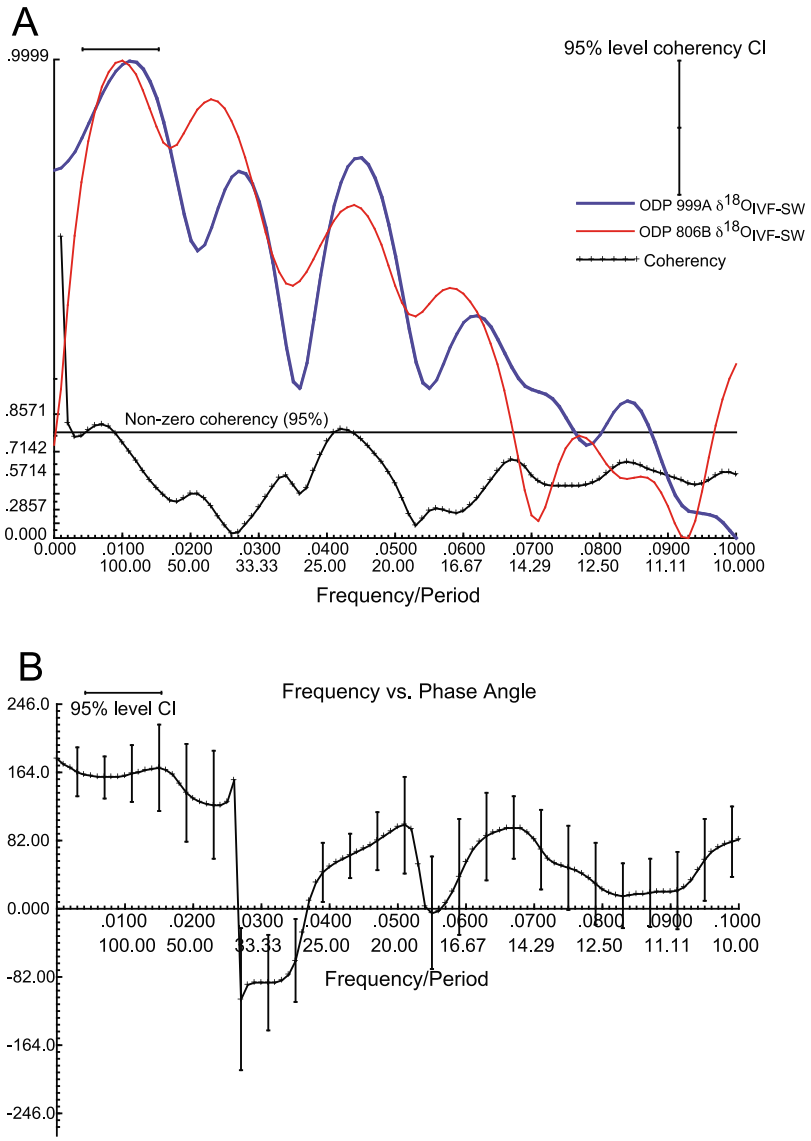

Figure 7. (a) Cross-spectral analysis of the individual ODP 999A and ODP 806B $\delta^{18}O_{IVF\text{-}SW}$ records and (b) the corresponding phase angle analysis. The cross correlation indicates coherency at the 100 and 23 kyr frequencies. Also note the phase angle at the 100 kyr frequency is out of phase and nearly 180° (within error) while the phase angle at 23 kyr is much smaller (between 10°–80°) and much closer to being in phase.

the 999A − 806B $\delta^{18}O_{IVF\text{-}SW}$ difference (Figure 6c). Further evidence for the phasing of the $\delta^{18}O_{IVF\text{-}SW}$ cycles between the two sites comes from the cross-correlation and phase angle analysis of the 999A and 806B $\delta^{18}O_{IVF\text{-}SW}$ records (Figure 7, based on the Arand package [*Howell*, 2001]). The cross-correlation analysis indicates statistically significant coherency between the two records at the 100 and 23 kyr frequencies. The phase angle at the 100 kyr frequency is nearly 180° (within error) and is therefore out of phase between the two sites. This explains the clear, glacial-interglacial $\delta^{18}O_{IVF\text{-}SW}$ shifts observed in Figure 4 and supports our conclusion that $\delta^{18}O_{IVF\text{-}SW}$ changes are out of phase between the two sites on glacial-interglacial time scales. Although wavelet analysis reveals spectral power at the 23 kyr frequency in each individual record, it is absent in the differenced record. The absence of the 23 kyr cycle in Figure 6c suggests that precessional changes are nearly in phase between the two sites. Phase angle analysis indicates the two $\delta^{18}O_{IVF\text{-}SW}$ records are more in phase at the 23 kyr frequency, indicating only a small, 2–3 kyr offset (Figure 7b). A possible mechanism to explain in phase precessional changes at the two sites is that the intensity of the ITCZ oscillated on 23 kyr cycles as perihelion shifted through the seasons, affecting the amplitude of the annual cycle. When perihelion occurred during boreal summer, the seasonal cycle was greatest and the ITCZ intensity at a maximum in

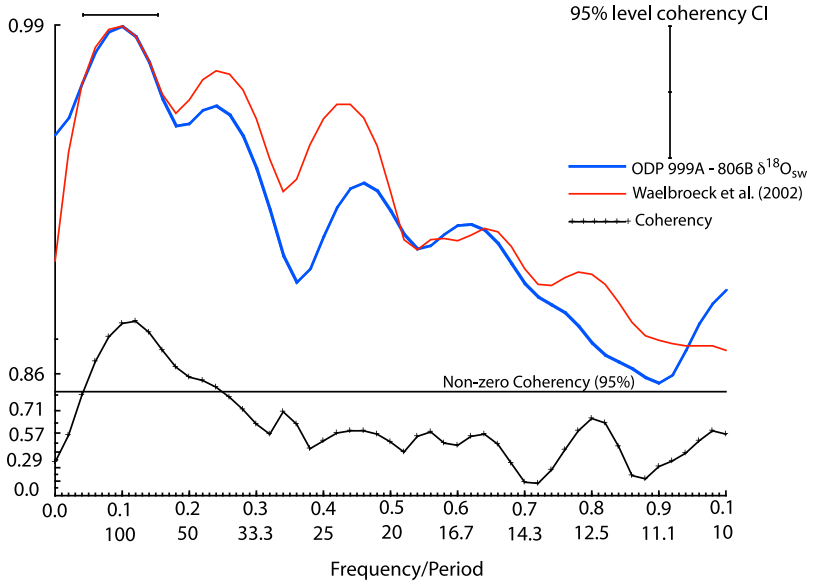

Figure 8. Cross-spectral analysis of the ODP 999A − ODP 806B $\delta^{18}O_{SW}$ difference and the global seawater $\delta^{18}O$ record of *Waelbroeck et al.* [2002] over the last 360 kyr, showing coherency between the two records at the 1/100 and 1/41 kyr frequencies and strong spectral power at all three of the major earth orbital periods of 23, 41, and 100 kyr.

the northern tropics. A more intense ITCZ during these periods probably resulted in more precipitation at both sites. Furthermore, the fact that the 23 kyr cycle is in phase and the 100 kyr cycle is out of phase between the two sites may explain why some of the higher-frequency (less than 100 kyr) $\delta^{18}O_{IVF\text{-}SW}$ oscillations shown on Figure 4 vary in phasing between the two sites.

[35] The second greatest spectral power in the 999A − 806B $\delta^{18}O_{IVF\text{-}SW}$ differenced record is at the 41 kyr frequency. The 41 kyr frequency is especially strong during the first 140 kyr and again after about 230 kyr. Because obliquity insolation changes are much greater at high latitudes [*Loutre et al.*, 2004], power at the 41 kyr frequency provides additional evidence for a high-latitude forcing mechanism.

[36] Application of cross-spectral analysis [*Howell*, 2001] between the 999A − 806B $\delta^{18}O_{SW}$ difference and the global $\delta^{18}O_{SW}$ record of *Waelbroeck et al.* [2002] reveals remarkable similarity between the two records (Figure 8) with strong spectral power in both records at all three of the major orbital frequencies: precession (23 kyr), obliquity (41 kyr) and eccentricity (100 kyr) (Figure 8). Furthermore, the two records are coherent (above the 95% confidence level) at the 100 and the 41 kyr frequencies. Although there is less coherency at the 23 kyr frequency, both records contain spectral power in the precessional band. The lack of strong coherence at the 23 kyr frequency could be due to age model error in the individual records. Furthermore, phase analysis reveals the 999A − 806B $\delta^{18}O_{SW}$ difference and the global $\delta^{18}O_{SW}$ record of *Waelbroeck et al.* [2002] are in phase (within error of 0° phase angle) at the 100 and 41 kyr frequencies. If we can assume the *Waelbroeck et al.* [2002] $\delta^{18}O_{SW}$ record primarily reflects changes in continental ice volume, cross-spectral analysis supports our conclusion that hydrologic variability between the Caribbean and the WEP are coherent and in phase with continental ice volume variability.

5. Conclusions

[37] Utilizing western Caribbean $\delta^{18}O_{SW}$ reconstructions, we demonstrate that the western tropical Atlantic experienced significant salinity changes on glacial-interglacial time scales over the last 360 kyr. Our results show that surface waters in the Caribbean became exceptionally salty during glacial periods, experiencing $\delta^{18}O_{SW}$ increases of 0.5 to 0.6‰ during glacial intervals. Our reconstruction of elevated surface salinities in the Caribbean during glacial episodes support a southward shift in the mean position of the glacial ITCZ during periods of reduced AMOC. A more southerly ITCZ combined with stronger glacial trade winds and a shift to more permanent El Niño–like conditions during glacial periods would result in a more arid western tropical Atlantic climate and an increase in atmospheric freshwater flux from the northern tropical Atlantic.

[38] Comparison of the Caribbean $\delta^{18}O_{SW}$ record over the past 360 kyr with a previously published record of $\delta^{18}O_{SW}$ change at Site 806B in the WEP shows systematic changes in the tropical east-west salinity gradient on glacial-interglacial time scales. During glacial periods, the Caribbean-WEP $\delta^{18}O_{SW}$ gradient increases, indicating the Caribbean becomes saltier as the WEP becomes fresher. The 999A − 806B $\delta^{18}O_{SW}$ difference covaries in both timing and magnitude with continental ice volume on glacial-interglacial times scales, indicating a greater salinity gradient existed between the Caribbean and western tropical Pacific during

glacial periods. Although wavelet analyses of the individual $\delta^{18}O_{IVF\text{-}SW}$ records indicate spectral power at all three major orbital frequencies, cross-spectral and phase angle analyses reveal the 100 kyr frequency is almost 180° out of phase between the two sites while the 23 kyr frequency is much closer to being in phase. This results in the development of a very large $\delta^{18}O_{SW}$ gradient between the western tropical Atlantic and the western equatorial Pacific on glacial-interglacial timescales. Even though this gradient is mapped over a large distance, these changes in surface $\delta^{18}O_{SW}$ provide indication of a southward migration of the glacial ITCZ during periods of reduced AMOC. A more southerly ITCZ combined with stronger glacial trade winds would result in a more arid western tropical Atlantic climate and a possible increased freshwater flux across the Central American isthmus.

[39] A southward shift in the glacial marine ITCZ may also increase the Atlantic-Pacific salinity gradient. Both numerical experiments using regional climate models [*Xie et al.*, 2008] as well as proxy evidence [*Pahnke et al.*, 2007] from the eastern equatorial Pacific suggests that a southward ITCZ shift increases the freshwater transport across the Central American Isthmus. Because the accumulation of excess salt in the tropical North Atlantic ultimately impacts the density of high-latitude surface waters, elevated salinity affects North Atlantic climate through its influence on AMOC. Amplification of AMOC associated with transitions into warm phases may therefore be critically dependent on the delivery of salty waters that accumulate in the Caribbean and in the subtropical north Atlantic gyre during cold periods. These results suggest that the tropical hydrologic cycle may act as an important feedback mechanism for conditioning the climate system for a return to interglacial conditions.

[40] **Acknowledgments.** We thank the Ocean Drilling Program (ODP) for core samples. This material is based on work supported by a JOI-ODP Schlanger Ocean Drilling Fellowship to M.W.S. and by the National Science Foundation under grants 0327060 and 0550703 to H.J.S. Additional funding was provided by the UC Davis Department of Geology Durrell Funds and by a UC Davis Humanities Fellowship to M.W.S. Laboratory assistance from D. Pak and numerous UC Davis undergraduate assistants and mass spectrometer operation by G. Paradis and D. Winter were critical to the success of this study. Elemental analyses were conducted in D. Lea's lab at UCSB. We also thank A. Droxler (Rice U.) for providing a suite of his ODP 999A samples, John Chiang (UC Berkeley) for valuable discussions, Ping Chang (TAMU) for assistance in the creation of Figure 6, and Kelly Cole (TAMU) for assistance with the wavelet analyses. This manuscript was also improved by the comments and suggestions by Brad Rosenheim and two additional anonymous reviewers.

References

Alexander, M., and J. Scott (2002), The influence of ENSO on air-sea interaction in the Atlantic, *Geophys. Res. Lett.*, *29*(14), 1701, doi:10.1029/2001GL014347.

Alexander, M. A., et al. (2002), The atmospheric bridge: The influence of ENSO teleconnections on air-sea interaction over the global oceans, *J. Clim.*, *15*, 2205–2231, doi:10.1175/1520-0442(2002)015<2205:TABTIO>2.0.CO;2.

Anand, P., H. Elderfield, and M. H. Conte (2003), Calibration of Mg/Ca thermometry in planktonic foraminifera from a sediment trap time series, *Paleoceanography*, *18*(2), 1050, doi:10.1029/2002PA000846.

Arbuszewski, J. A., et al. (2009), Towards a global calibration of the *G. ruber* (white) Mg/Ca paleothermometer, *Geochim. Cosmochim. Acta, Suppl.*, *73*(13), A49.

Bassinot, F. C., et al. (1994), The astronomical theory of climate and the age of the Brunhes-Matuyama magnetic reversal, *Earth Planet. Sci. Lett.*, *126*, 91–108, doi:10.1016/0012-821X(94)90244-5.

Bemis, B. E., H. J. Spero, J. Bijma, and D. W. Lea (1998), Reevaluation of the oxygen isotopic composition of planktonic foraminifera: Experimental results and revised paleotemperature equations, *Paleoceanography*, *13*, 150–160, doi:10.1029/98PA00070.

Broccoli, A. J., K. A. Dahl, and R. J. Stouffer (2006), Response of the ITCZ to Northern Hemisphere cooling, *Geophys. Res. Lett.*, *33*, L01702, doi:10.1029/2005GL024546.

Bush, A. B. G. (2007), Extratopical influences on the El Nino-Southern Oscillation through the Late Quaternary, *J. Clim.*, *20*, 788–800, doi:10.1175/JCLI4048.1.

Bush, A. G., and S. H. Philander (1998), The role of ocean-atmosphere interactions in tropical cooling during the last glacial maximum, *Science*, *279*, 1341–1344, doi:10.1126/science.279.5355.1341.

Cane, M. A. (1998), A role for the Tropical Pacific, *Science*, *282*, 59–61, doi:10.1126/science.282.5386.59.

Cane, M., and A. C. Clement (1999), A role for the tropical Pacific coupled ocean-atmosphere system on Milankovich and millennial timescales Part II: Global impacts, in *Mechanisms of Global Climate Change at Millennial Time Scales*, *Geophys. Monogr. Ser.*, vol. 112, edited by P. U. Clark, R. S. Webb, and L. D. Keigwin, pp. 373–384, AGU, Washington, D. C.

Carlson, A. E., et al. (2008), Subtropical Atlantic salinity variability and Atlantic meridional circulation during the last deglaciation, *Geology*, *36*, 991–994, doi:10.1130/G25080A.1.

Chen, B., et al. (2008), Frequency distribution of daily ITCZ patterns over the western-central Pacific, *J. Clim.*, *21*, 4207–4222, doi:10.1175/2008JCLI1973.1.

Chiang, J. C. H., and C. M. Bitz (2005), Influence of high latitude ice cover on the marine Intertropical Convergence Zone, *Clim. Dyn.*, *25*, 477–496, doi:10.1007/s00382-005-0040-5.

Chiang, J. C. H., M. Biasutti, and D. S. Battisti (2003), Sensitivity of the Atlantic Intertropical Convergence Zone to Last Glacial Maximum boundary conditions, *Paleoceanography*, *18*(4), 1094, doi:10.1029/2003PA000916.

Clement, A. C., and M. Cane (1999), A role for the Tropical Pacific coupled ocean-atmosphere system on Milankovitch and millennial timescales. Part I: A modeling study of Tropical Pacific variability, in *Mechanisms of Global Climate Change at Millennial Time Scales*, *Geophys. Monogr. Ser.*, vol. 112, edited by P. U. Clark, R. S. Webb, and L. D. Keigwin, pp. 363–372, AGU, Washington, D. C.

Clement, A. C., R. Seager, and M. A. Cane (1999), Orbital controls on the El Niño/Southern Oscillation and the tropical climate, *Paleoceanography*, *14*, 441–456, doi:10.1029/1999PA900013.

Conkright, M. E., et al. (2002), *World Ocean Atlas 2001: Objective Analyses, Data Statistics, and Figures* [CD-ROM], 17 pp., Natl. Oceanogr. Data Cent., Silver Spring, Md.

Cruz, F. W., et al. (2005), Insolation-driven changes in atmospheric circulation over the past 116,000 years in subtropical Brazil, *Nature*, *434*, 63–66, doi:10.1038/nature03365.

Curry, R., B. Dickson, and I. Yashayaev (2003), A change in the freshwater balance of the Atlantic Ocean over the past four decades, *Nature*, *426*, 826–829, doi:10.1038/nature02206.

Dahl, K., et al. (2005), Assessing the role of North Atlantic freshwater forcing in millennial scale climate variability: A tropical Atlantic perspective, *Clim. Dyn.*, *24*, 325–346, doi:10.1007/s00382-004-0499-5.

Dekens, P. S., D. W. Lea, D. K. Pak, and H. J. Spero (2002), Core top calibration of Mg/Ca in tropical foraminifera: Refining paleotemperature estimation, *Geochem. Geophys. Geosyst.*, *3*(4), 1022, doi:10.1029/2001GC000200.

Delcroix, T., and M. McPhaden (2002), Interannual sea surface salinity and temperature changes in the western Pacific warm pool during 1992–2000, *J. Geophys. Res.*, *107*(C12), 8002, doi:10.1029/2001JC000862.

Delcroix, T., and J. Picaut (1998), Zonal displacement of the western equatorial Pacific fresh pool, *J. Geophys. Res.*, *103*, 1087–1098, doi:10.1029/97JC01912.

Dong, B., and R. T. Sutton (2007), Enhancement of ENSO variability by a weakened Atlantic thermohaline circulation in a coupled GCM, *J. Clim.*, *20*, 4920–4939, doi:10.1175/JCLI4284.1.

Dürkoop, A., W. Hale, S. Mulitza, J. Pätzold, and G. Wefer (1997), Late Quaternary variations of sea surface salinity and temperature in the western tropical Atlantic: Evidence from $\delta^{18}O$ of *Globigerinoides sacculifer*, *Paleoceanography*, *12*, 764–772, doi:10.1029/97PA02270.

Dykoski, C. A., et al. (2005), A high-resolution, absolute-dated Holocene and deglacial Asian

monsoon record from Dongge Cave, China, *Earth Planet. Sci. Lett.*, *233*, 71–86, doi:10.1016/j.epsl.2005.01.036.

Eggins, S. M., et al. (2004), Modulation and daily banding of Mg/Ca in Orbulina universa tests by symbiont photosynthesis and respiration: A complication for seawater thermometry?, *Earth Planet. Sci. Lett.*, *225*, 411–419, doi:10.1016/j.epsl.2004.06.019.

Ferguson, J. E., et al. (2008), Systematic change of foraminiferal Mg/Ca ratios across a strong salinity gradient, *Earth Planet. Sci. Lett.*, *265*, 153–166, doi:10.1016/j.epsl.2007.10.011.

Giannini, A., et al. (2001), The ENSO teleconnection to the tropical Atlantic Ocean: Contributions of the remote and local SSTs to rainfall variability in the tropical Americas, *J. Clim.*, *14*, 4530–4544, doi:10.1175/1520-0442(2001)014<4530:TETTTT>2.0.CO;2.

Hastenrath, S. (2002), The intertropical convergence zone of the eastern Pacific revisited, *Int. J. Climatol.*, *22*, 347–356, doi:10.1002/joc.739.

Hoogakker, B. A. A., et al. (2009), Mg/Ca paleothermometry in high salinity environments, *Earth Planet. Sci. Lett.*, *284*, 583–589, doi:10.1016/j.epsl.2009.05.027.

Howell, P. (2001), ARAND time series and spectral analysis package for the Macintosh, Brown University, *IGBP PAGES/World Data Cent. for Paleoclimatol. Data Contrib. Ser. 2001-044*, Natl. Clim. Data Cent., Boulder, Colo.

Kameo, K., et al. (2004), Glacial-interglacial surface water variations in the Caribbean Sea during the last 300 ky based on calcareous nannofossil analysis, *Palaeogeogr. Palaeoclimatol. Palaeoecol.*, *212*, 65–76.

Kawahata, H., et al. (2002), Seasonal change in foraminiferal production in the western equatorial Pacific warm pool: Evidence from sediment trap experiments, *Deep Sea Res., Part II*, *49*(13–14), 2783–2800, doi:10.1016/S0967-0645(02)00058-9.

Koutavas, A., and J. Lynch-Stieglitz (2003), Glacial-interglacial dynamics of the eastern equatorial Pacific cold tongue Intertropical Convergence Zone system reconstructed from oxygen isotope records, *Paleoceanography*, *18*(4), 1089, doi:10.1029/2003PA000894.

Koutavas, A., et al. (2002), El Nino-like pattern in Ice Age tropical Pacific sea surface temperature, *Science*, *297*, 226–230, doi:10.1126/science.1072376.

Kukla, G., et al. (2002), Last interglacial and early glacial ENSO, *Quat. Res.*, *58*, 27–31, doi:10.1006/qres.2002.2327.

Latif, M., et al. (2000), Tropical stabilization of the thermohaline circulation in a greenhouse warming simulation, *J. Clim.*, *13*, 1809–1813, doi:10.1175/1520-0442(2000)013<1809:L>2.0.CO;2.

Lea, D. W., and P. A. Martin (1996), A rapid mass spectrometric method for the simultaneous analysis of barium, cadmium, and strontium in foraminifera shells, *Geochim. Cosmochim. Acta*, *60*(16), 3143–3149, doi:10.1016/0016-7037(96)00184-6.

Lea, D. W., et al. (1999), Controls on magnesium and strontium uptake in planktonic foraminifera determined by live culturing, *Geochim. Cosmochim. Acta*, *63*(16), 2369–2379, doi:10.1016/S0016-7037(99)00197-0.

Lea, D. W., et al. (2000), Climate impact of Late Quaternary equatorial Pacific sea surface temperature variations, *Science*, *289*, 1719–1724, doi:10.1126/science.289.5485.1719.

Lea, D. W., et al. (2003), Synchrononeity of tropical high latitude Atlantic temperatures over the last glacial termination, *Science*, *301*, 1361–1364, doi:10.1126/science.1088470.

LeGrande, A. N., and G. A. Schmidt (2009), Sources of Holocene variability of oxygen isotopes in paleoclimate archives, *Clim. Past*, *5*(3), 441–455, doi:10.5194/cp-5-441-2009.

Lohmann, G. (2003), Atmospheric and oceanic freshwater transport during weak Atlantic overturning circulation, *Tellus, Ser A.*, *55*, 438–449.

Lohmann, G., and S. Lorenz (2000), The water cycle under paleoclimatic conditions as derived from AGCM simulations, *J. Geophys. Res.*, *105*, 17,417–17,436, doi:10.1029/2000JD900189.

Loutre, M. F., et al. (2004), Does mean annual insolation have the potential to change the climate?, *Earth Planet. Sci. Lett.*, *221*, 1–14, doi:10.1016/S0012-821X(04)00108-6.

Lund, D. C., and W. Curry (2006), Florida Current surface temperature and salinity variability during the last millennium, *Paleoceanography*, *21*, PA2009, doi:10.1029/2005PA001218.

Magaña, V., et al. (1999), The midsummer drought over Mexico and Central America, *J. Clim.*, *12*, 1577–1588, doi:10.1175/1520-0442(1999)012<1577:TMDOMA>2.0.CO;2.

Mashiotta, T. A., et al. (1999), Glacial-interglacial changes in subantarctic sea surface temperature and δ^{18}O-water using foraminiferal Mg, *Earth Planet. Sci. Lett.*, *170*, 417–432, doi:10.1016/S0012-821X(99)00116-8.

Mora, G., and J. I. Martinez (2005), Sedimentary metal ratios in the Colombia Basin as indicators for water balance change in northern South America during the past 400,000 years, *Paleoceanography*, *20*, PA4013, doi:10.1029/2005PA001132.

Nürnberg, D., et al. (2008), Interacting loop current variability and Mississippi River discharge over the past 400 kyr, *Earth Planet. Sci. Lett.*, *272*, 278–289, doi:10.1016/j.epsl.2008.04.051.

Oppo, D. W., et al. (2009), 2,000-year-long temperature and hydrology reconstructions from the Indo-Pacific warm pool, *Nature*, *460*, 1113–1116, doi:10.1038/nature08233.

Pahnke, K., J. P. Sachs, L. Keigwin, A. Timmermann, and S.-P. Xie (2007), Eastern tropical Pacific hydrologic changes during the past 27,000 years from D/H ratios in alkenones, *Paleoceanography*, *22*, PA4214, doi:10.1029/2007PA001468.

Paillard, D., L. Labeyrie, and P. Yiou (1996), Macintosh program performs time-series analysis, *Eos Trans. AGU*, *77*(39), F379, doi:10.1029/96EO00259.

Partin, J. W., et al. (2007), Millennial-scale trends in west Pacific warm pool hydrology since the Last Glacial Maximum, *Nature*, *449*, 452–453, doi:10.1038/nature06164.

Peterson, L. C., et al. (2000), Rapid changes in the hydrologic cycle of the tropical Atlantic during the last Glacial, *Science*, *290*, 1947–1951, doi:10.1126/science.290.5498.1947.

Poveda, G., and O. J. Mesa (1997), Feedbacks between hydrological processes in tropical South America and large-scale ocean-atmospheric phenomena, *J. Clim.*, *10*, 2690–2702, doi:10.1175/1520-0442(1997)010<2690:FBHPIT>2.0.CO;2.

Poveda, G., and O. J. Mesa (2000), On the existence of Lloro (the rainiest locality on Earth): Enhanced ocean-land-atmosphere interaction by a low-level jet, *Geophys. Res. Lett.*, *27*, 1675–1678, doi:10.1029/1999GL006091.

Poveda, G., et al. (2006), Annual and inter-annual variability of the present climate in northern South America and southern Mesoamerica, *Palaeogeogr. Palaeoclimatol. Palaeoecol.*, *234*, 3–27, doi:10.1016/j.palaeo.2005.10.031.

Roche, D., et al. (2004), Oceanic oxygen-18 at the present day and LGM: Equilibrium simulations with a coupled climate model of intermediate complexity, *Earth Planet. Sci. Lett.*, *218*, 317–330, doi:10.1016/S0012-821X(03)00700-3.

Sachs, J. P., et al. (2009), Southward movement of the Pacific intertropical convergence zone AD 1400–1850, *Nat. Geosci.*, *2*, 519–525, doi:10.1038/ngeo554.

Sadekov, A., S. M. Eggins, P. De Deckker, and D. Kroon (2008), Uncertainties in seawater thermometry deriving from intratest and intertest Mg/Ca variability in *Globigerinoides ruber*, *Paleoceanography*, *23*, PA1215, doi:10.1029/2007PA001452.

Sadekov, A., S. M. Eggins, P. De Deckker, U. Ninnemann, W. Kuhnt, and F. Bassinot (2009), Surface and subsurface seawater temperature reconstruction using Mg/Ca microanalysis of planktonic foraminifera *Globigerinoides ruber, Globigerinoides sacculifer*, and *Pulleniatina obliquiloculata*, *Paleoceanography*, *24*, PA3201, doi:10.1029/2008PA001664.

Schmidt, M. W., et al. (2004), Links between salinity variation in the Caribbean and North Atlantic thermohaline circulation, *Nature*, *428*, 160–163, doi:10.1038/nature02346.

Schmidt, M. W., M. J. Vautravers, and H. J. Spero (2006a), Western Caribbean sea surface temperatures during the late Quaternary, *Geochem. Geophys. Geosyst.*, *7*, Q02P10, doi:10.1029/2005GC000957.

Schmidt, M. W., M. J. Vautravers, and H. J. Spero (2006b), Rapid subtropical North Atlantic salinity oscillations across Dansgaard-Oeschger cycles, *Nature*, *443*, 561–564, doi:10.1038/nature05121.

Schmittner, A., and A. C. Clement (2002), Sensitivity of the thermohaline circulation to tropical and high latitude freshwater forcing during the last glacial- interglacial cycle, *Paleoceanography*, *17*(2), 1017, doi:10.1029/2000PA000591.

Schmittner, A., C. Appenzeller, and T. F. Stocker (2000), Enhanced Atlantic freshwater export during El Niño, *Geophys. Res. Lett.*, *27*(8), 1163–1166, doi:10.1029/1999GL011048.

Spero, H. J., S. Eggins, A. Russell, L. Vetter, and B. Hoenisch (2008), Experimental perspective on cause and impact of planktonic foraminifera intrashell Mg/Ca variability on paleoceanographic applications, *Eos Trans. AGU*, *89*(53), Fall Meet. Suppl., Abstract PP41F-01.

Stidd, C. K. (1967), The use of eigenvectors for climate estimates, *J. Appl. Meteorol.*, *6*, 255–264, doi:10.1175/1520-0450(1967)006<0255:TUOEFC>2.0.CO;2.

Stott, L. D., et al. (2002), Super ENSO and global climate oscillations at millennial time scales, *Science*, *297*, 222–226, doi:10.1126/science.1071627.

Stouffer, R. J., et al. (2006), Investigating the causes of the response of the thermohaline circulation to past and future climate changes, *J. Clim.*, *19*, 1365–1387, doi:10.1175/JCLI3689.1.

Thunell, R., et al. (1999), Sea-surface temperature anomalies associated with the 1997–1998 El Nino recorded in the oxygen isotope

composition of planktonic foraminifera, *Geology*, *27*(9), 843–846, doi:10.1130/0091-7613(1999)027<0843:SSTAAW>2.3.CO;2.

Tierney, J. E., D. W. Oppo, Y. Rosenthal, J. M. Russell, and B. K. Linsley (2010), Coordinated hydrological regimes in the Indo-Pacific region during the past two millennia, *Paleoceanography*, *25*, PA1102, doi:10.1029/2009PA001871.

Torrence, C., and G. P. Compo (1998), A practical guide to wavelet analysis, *Bull. Am. Meteorol. Soc.*, *79*(1), 61–78, doi:10.1175/1520-0477(1998)079<0061:APGTWA>2.0.CO;2.

Vellinga, M., and R. A. Wood (2002), Global climatic impacts of a collapse of the Atlantic thermohaline circulation, *Clim. Change*, *54*, 251–267, doi:10.1023/A:1016168827653.

Vellinga, M., and P. L. Wu (2004), Low-latitude freshwater influence on centennial variability of the Atlantic thermohaline circulation, *J. Clim.*, *17*, 4498–4511, doi:10.1175/3219.1.

Waelbroeck, C., et al. (2002), Sea-level and deep water temperature changes derived from benthic foraminifera isotopic records, *Quat. Sci. Rev.*, *21*, 295–305, doi:10.1016/S0277-3791(01)00101-9.

Wang, X. F., et al. (2004), Wet periods in northeastern Brazil over the past 210 kyr linked to distant climate anomalies, *Nature*, *432*, 740–743, doi:10.1038/nature03067.

Wang, X. F., et al. (2006), Interhemispheric antiphasing of rainfall during the last glacial period, *Quat. Sci. Rev.*, *25*, 3391–3403, doi:10.1016/j.quascirev.2006.02.009.

Wang, Y. J., et al. (2001), A high-resolution absolute-dated Late Pleistocene monsoon record from Hulu Cave, China, *Science*, *294*, 2345–2348, doi:10.1126/science.1064618.

Watanabe, T. A., et al. (2001), Seasonal changes in sea surface temperature and salinity during the Little Ice Age in the Caribbean Sea deduced from Mg/Ca and 18O/16O ratios in corals, *Mar. Geol.*, *173*, 21–35, doi:10.1016/S0025-3227(00)00166-3.

Weldeab, S., et al. (2006), Deglacial sea surface temperature and salinity increase in the western tropical Atlantic in synchrony with high latitude climate instabilities, *Earth Planet. Sci. Lett.*, *241*, 699–706, doi:10.1016/j.epsl.2005.11.012.

Xie, S. P., et al. (2008), Influences of Atlantic climate change on the tropical Pacific via the Central American Isthmus, *J. Clim.*, *21*, 3914–3928, doi:10.1175/2008JCLI2231.1.

Yarincik, K. M., R. W. Murray, and L. C. Peterson (2000), Climatically sensitive eolian and hemipelagic deposition in the Cariaco Basin, Venezuela, over the past 578,000 years: Results from Al/Ti and K/Al, *Paleoceanography*, *15*(2), 210–228, doi:10.1029/1999PA900048.

Yuan, D., et al. (2004), Timing, duration and transitions of the last interglacial Asian monsoon, *Science*, *304*, 575–578, doi:10.1126/science.1091220.

Zhang, R., and T. L. Delworth (2005), Simulated Tropical response to a substantial weakening of the Atlantic thermohaline circulation, *J. Clim.*, *18*, 1853–1860, doi:10.1175/JCLI3460.1.

M. W. Schmidt, Department of Oceanography, Texas A&M University, 1204 O&M Bldg., College Station, TX 77843, USA. (schmidt@ocean.tamu.edu)

H. J. Spero, Department of Geology, University of California Davis, 1 Shields Ave., Davis, CA 95616, USA. (hjspero@ucdavis.edu)